PAPER

Check for updates

Facile covalent functionalization of boron nitride nanotubes *via* coupling reaction†

Thang Quoc Huynh, [ID] [ab] Minsung Kang, [ID] [a] Jeung Gon Kim [ID] *[bc] and Seokhoon Ahn [ID] *[ac]

A broad range of functionalized boron nitride nanotubes has been synthesized using a facile method based on the coupling reaction between BNNT and arenediazonium tetrafluoroborate derivatives. The formation of covalent bonds between nanotubes and organic moieties results in homogeneous dispersions in organic solvents, such as *N,N'*-dimethylformamide, acetone, isopropanol, and tetrahydrofuran. Digital images demonstrated improved and stabilized dispersions lasting for several days, while TEM analysis indicated no breakdown of nanotubes due to the mild reaction conditions employed. The functionalization process was further confirmed through additional characterization, employing FTIR, XPS, and TGA. Surface-functionalized materials exhibited a significant weight percentage of functionality, reaching up to 21.8% according to TGA.

Introduction

Boron nitride nanotubes (BNNT) are one-dimensional structures of boron nitride that were theoretically predicted in 1994,[1] and then experimentally discovered in 1995.[2] They are cylinders with nanometer-scale diameters and micrometer lengths alternately composed of nitrogen and boron atoms and arranged in a hexagonal lattice.[3] The nanotubes have extremely remarkable physical characteristics due to their low dimensionality and high surface area-to-volume ratio. BNNT are broadband gap semiconductors unaffected by tube radius, chirality, or other geometrical parameters.[4] They offer outstanding mechanical qualities,[5–8] high thermal conductivity,[9,10] excellent electrical insulator characteristics,[11–13] oxidation resistance,[14] and chemical stability,[15] making them particularly advantageous in devices operating in hazardous and high-temperature settings.[3,4,16] Not surprisingly, studies on the properties and uses of this exotic material have attracted a lot of attention due to its excellent qualities. Over the last decades, many applications have relied on BNNT including high thermal conductivity,[17–22] thermal stability,[23] synthetic biology,[24–26] aerospace,[27] electrical technology,[28,29] biomedical materials,[30–32] optical materials,[33,34] and even power generation.[35]

In spite of material potential, there are still critical issues preventing them from further applications. Due to insolubility and inert-chemical reactivity, the tubes are super difficult to disperse and distribute uniformly in fabricating systems.[36,37] Inadequate dispersion, aggregation, and bundling frequently have adverse effects on the inherent characteristics, resulting in considerably reduced values compared to what is theoretically anticipated. To illustrate, subpar dispersion can hinder the efficient transfer of loads from the matrix to nanotube reinforcements within a composite material, leading to a deterioration in the structural mechanical properties. Achieving effective dispersion and comprehending the interplay between matrix chemistry, manufacturing techniques, and the resultant physical attributes are essential for customizing nanocomposite materials' performance.[38] Hence, the capacity to manipulate BNNT within uniform and consistent solutions empowers researchers to tap into their unique and advantageous properties, facilitating fundamental investigations.

To tackle this issue, various chemical techniques have been explored for functionalizing and dispersing BNNT, with most employing harsh acids to oxidize B–N bonds or resorting to more sophisticated or unconventional reduction techniques.[15,39–41] Covalent bonding through aggressive chemical reactions damages the outer wall of BNNT, thereby compromising their intrinsic properties. In contrast, gas-phase surface modification techniques like ammonia plasma and chemical vapor deposition (CVD) can address some issues while minimizing the loss of BNNT's unique properties, but with low reaction efficiency.[42,43] Consequently, several challenges remain unaddressed, which concerns the absence of an effective method to graft a high density of functional groups onto BNNT,

[a]Institute of Advanced Composite Materials, Korea Institute of Science and Technology (KIST), Chudong-ro 92, Bongdong-eup, Wanju-gun 55324, Jeonbuk, Korea. E-mail: ahn75@kist.re.kr

[b]Department of Chemistry and Research Institute of Physics and Chemistry, Jeonbuk National University, Jeonbuk 54896, Republic of Korea. E-mail: jeunggonkim@jbnu.ac.kr

[c]Department of JBNU-KIST Industry-Academia Convergence Research, Jeonbuk National University, Jeonbuk 54896, Republic of Korea

† Electronic supplementary information (ESI) available. See DOI: https://doi.org/10.1039/d4na00458b

rendering them chemically active and enabling more efficient surface modification.

In this study, we propose a method that avoids the use of strong acids, potent oxidizing agents, toxic reagents, or metallic materials. The reaction conditions involve only mild heating and are very easy to handle, ensuring the preservation of the nanotubes and the absence of any broken signals, resulting high degree of functionalization of up to 21.8 wt% with the possibility to scale up which is far better than previous reports.[44–48] To understand the mechanism, the hypothesis that a highly active intermediate product generated from diazonium salt interacted with the B-active position on the surface of BNNT was suggested by XPS characterization.

Results and discussion

Reaction development, characterization, and mechanism proposal

Diazonium salts are a category of organic compounds featuring a common functional group $R-N^{2+}X^-$, where R represents an organic component (like alkyl or aryl groups), and X signifies an organic or inorganic anion (e.g., a halogen, BF^{4-}). These compounds are recognized as high-energy materials capable of undergoing violent decomposition upon heating or exposure to mechanical force (shock-sensitive) that produce an aryl radical as a super-reactive intermediate product. These salts have been effectively employed in various transformations, particularly with low-dimensional materials like carbon nanotubes (CNT).[49,50] Inspired by the previous achievement, we anticipate that the highly reactive intermediate can engage with BNNT by donating electrons to the boron center, which has naturally low electron density. Consequently, 2f was chosen as a model substrate for modification of BNNT surface because it was well-known as a strong reactive reagent compared to other salts (detailed reaction scheme and structure of all salts was depicted in Fig. 1). We systematically optimized reaction conditions, and these examples were selected in ESI Table 1.† There were solvent systems that have been examined to identify a suitable environment for the reaction as we expected. Exploitation of common solvents such as water in ethanol, water, ethanol, or acetone (ESI Table 1,† samples 1–4) provided the desired product. However, with a low percentage of carbon atoms according to scanning from XPS, it was still an unsatisfactory transformation. Interestingly, employing $CHCl_3$ (ESI Table 1,† sample 5) provided the best results for this transformation, the amount of carbon atom dramatically increased to 20.69% compared to the other which was just under 10.51%. Thus,

$CHCl_3$ was selected as the solvent for further reaction. The addition of salt did not greatly improve the efficiency, unfortunately, it decreased of carbon atom percentage by 10.24%. A similar problem was caught up when the working temperature and reaction time increased (ESI Table 1,† sample 6–8). The resulting product (optimized sample, entry 5, ESI Table 1†), denoted as 3f, was then comprehensively characterized.

The primary concern pertains to preserving the integrity of the nanotubes during the reaction. This aspect holds significant importance since maintaining the structural integrity of the nanotubes is synonymous with safeguarding their valuable properties. To assess the preservation of nanotube structure, TEM analysis was employed. The results from this analysis revealed that the structure of BNNT remained intact. Importantly, there was no notable unzipping observed, and there was no discernible increase in BN nanosheet or nanoribbon content, as evidenced by the representative TEM images in Fig. 2a and b (before the reaction) and Fig. 2c and d (post-reaction). After grafting, amorphous organic coating layers might be observed on the nanotube surfaces, introducing a rough surface of 3f (Fig. 2d). These findings may not only suggest that the process (including the reaction and sonication process) did not significantly alter the structure of BNNT but also introduce an organic component to their surfaces. The TEM analysis provides valuable insights into the effects of reaction conditions on BNNT, highlighting their stability and robustness.

Further investigation was utilized, Fig. 3a and b demonstrated FTIR spectra of BNNT and 3f. The analysis revealed the observation of starting BNNT used in this experiment having B–N (in-plane) stretching at 1374 cm^{-1}, and B–N–B (out-of-plane) bending at 811 cm^{-1}, and 795 cm^{-1}. The shoulder at around 1100 cm^{-1} proved the existence of B–O stretch, and no C–H stretching was presented in the range 2950–2800 cm^{-1}. Considering the FTIR profile of 3f, witnessed the noticeable appearance of C–H stretching at around 2950–2800 cm^{-1} proves the presence of the aromatic ring on the BNNT surface. The magnification of

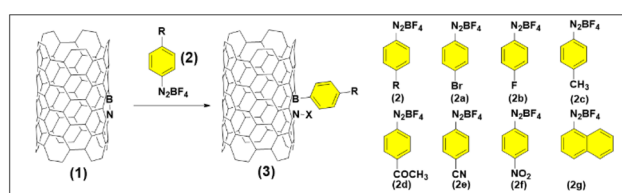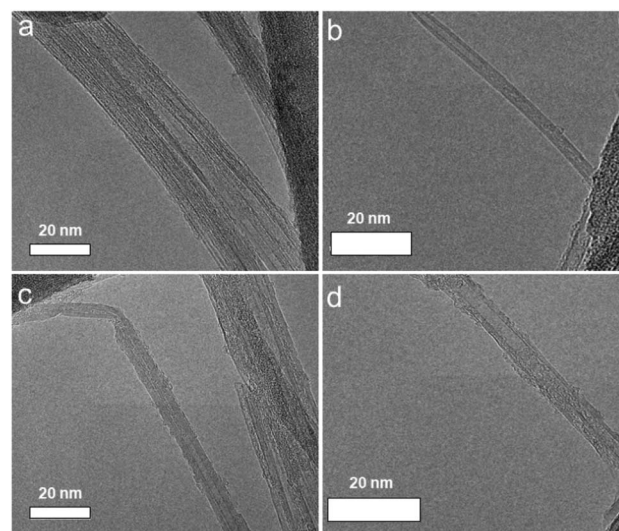Fig. 2 (a and b) TEM images of BNNTs – before reaction and (c and d) TEM images of 3f – after reaction.

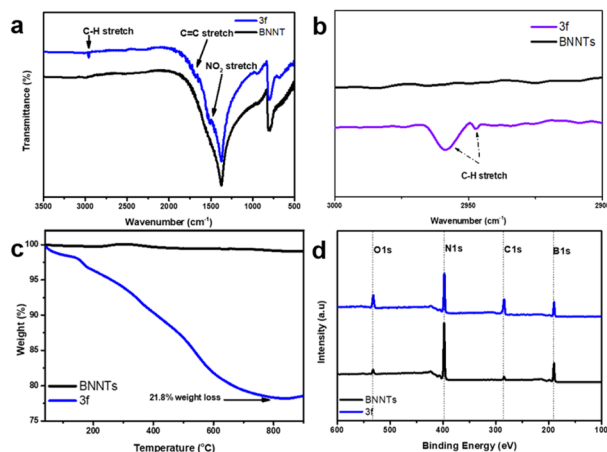Fig. 1 Reaction scheme and materials used in this study.

Fig. 3 (a) FTIR (b) FTIR magnified region (c) TGA (d) wide scan XPS of BNNTs and 3f.

the bracketed region shows in detail the peak position at around 2950 cm^{-1} of sample 3f indicating the appearance of C–H stretching from the phenyl group. In addition, the broad and weak from 1650–1400 cm^{-1} is a piece of evidence about the stretching of C=C, NO$_2$, and scissoring of C–H bond.

Thermogravimetric analysis (TGA) was used to quantify the degree of functionalization and determine the stability of both BNNT and functionalization products. This method involves comparing the breakdown temperatures of the nanotubes themselves to those of the species covalently bound to the surfaces of the tubes, which detach, decompose, or oxidize at lower temperatures. BNNT are known to be quite thermally stable, undergoing oxidation at extreme temperatures exceeding 800 °C. Hence, according to the TGA curves (Fig. 3c), it was observed that there was minimal heat loss exhibited by BNNT, which demonstrates the remarkable thermal stability of the structure of BNNT. Thermal stability of 3f samples from the reaction was also examined by TGA under air, the mass loss of sample 3f might be resulted from organic components, proving the existence of organic substances. Weight losses were observed under 200 °C, which may be the result of the removal of solvent absorbed inside nanotubes or some organic residues still present in the sample. From 200 °C to 800 °C, the spectra showed major mass changes of up to 21.8 wt% by the detachment or oxidation of a benzene ring grafted onto the surface of the nanotube during the functionalization reaction, indicating that a high level of functionalization was achieved and the reactivity of BNNT had been greatly enhanced by covalent bonds.

X-ray photoelectron spectroscopy (XPS) was performed to evaluate the effectiveness of functionalization in the case of element composition (Fig. 3d). The XPS wide-scan spectra of both the pristine BNNT and the functionalized BNNT 3f were compared in Fig. 3d, and their element content data were analyzed and summarized in ESI Table 3.† The results showed a significant decrease in the peak intensity of B 1s and N 1s in the functionalized BNNT, suggesting a reduction in the detectable levels of boron and nitrogen elements due to the presence of a grafting layer on the surface of BNNT.

Additionally, an increase in the percentage of carbon atoms was observed in the modified samples 22.44%. Increasing carbon content indicated the presence of a carbon substance, specifically aromatic rings, on the surface of BNNT after modification. This value is comparable to the TGA analysis mentioned above, the correlation between the two methods may result in a higher degree of consistency and comparability of the results obtained from different characterization techniques.

Fig. 4 illustrates the B 1s photoelectron spectroscopy results for BNNT and 3f. In both spectra, a common peak at 190.3 eV was identified, corresponding to the B–N bonding in pristine BNNT. Another similar peak at 191.5 eV, indicative of B–O, was observed in peak-fitting analysis, likely arising from residual B$_2$O$_3$ from the purification process. The 3f spectra revealed an additional peak at 190.8 eV, potentially attributed to the –B–C– bond, this peak offered valuable insights into the formation of 3f and the underlying reaction mechanism. In addition, analyzing the C 1s spectra of BNNT, a weak signal was detected in both BNNT and 3f, likely stemming from carbon contamination in the raw materials or equipment. In the 3f spectra, three other main peaks were noted, corresponding to the C–C, C–B, and C–N groups. The presence of the B–C peak (B 1s) and C–B peak (C 1s) strongly suggested that the diazonium salt had reacted with the B sites on the BNNT's surface.

The pieces of evidence from XPS analysis led us to propose a mechanism that gives us a better understanding of this reaction. We believe that the reaction starts with the formation of an electron donor–acceptor (EDA) complex between lone pair electrons of N-active position and aryl diazonium salt under accelerating heating (as depicted in Fig. 5).[51] Next, an EDA complex triggers a single electron transfer to generate aryl radical, which then directly forms a bond with BNNT by connecting with the B-active site through attack to p-orbital, affording radical intermediate **. The arene-functionalized nanotube may already exist as the delocalized radical cation, which may also accept electrons from nearby nanotubes or interact with fluoride or diazonium salts.[52]
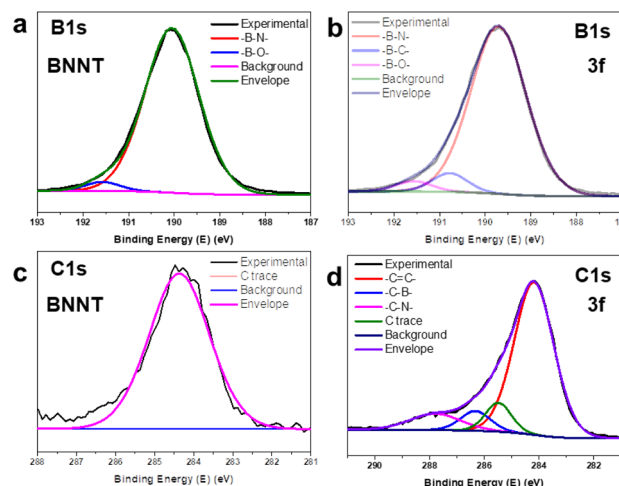

Fig. 4 The B 1s and C 1s core level spectra of (a and c) BNNT and (b and d) 3f.
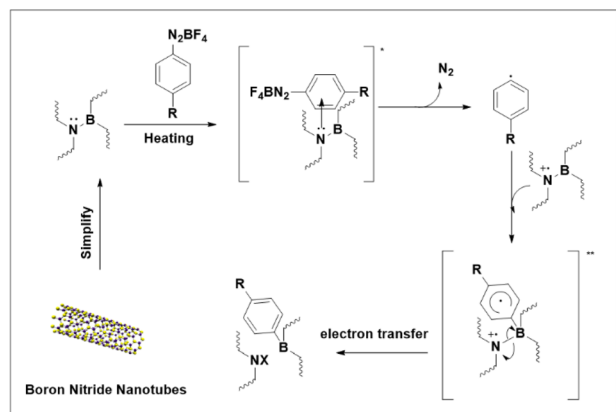
Fig. 5 Plausible mechanism of covalent functionalization of BNNT using diazonium salts.

Substrate scope, general dispersion evaluation

With the optimized reaction conditions in hand, we proceeded to investigate the range of substrates applicable to the synthesis of functionalized BNNT. Notably, this process exhibited remarkable tolerance when exposed to an array of aryl diazonium salts (Fig. 6).

To be more specific, aryl diazonium salts featuring a range of substituents were examined for their impact on product yield, as determined by TGA analysis (ESI Fig. 2 and Table 4†). These substituents included halogen groups (3a, 3b), electron-donating groups (3c), electron-withdrawing groups (3d, 3e, 3f), and electron-neutral groups (3g). Notably, a discernible electronic effect of these substituents was observed. Salts with electron-donating groups, like CH_3, displayed reduced reactivity, resulting in lower functionality, with a yield of only 4.1 wt%. Conversely, reactants with electron-withdrawing groups, such as $-COCH_3$ (11.8 wt%) and $-CN$ (11.8 wt%), exhibited notably higher functionality. In particular, the NO_2 group, known for its strong electron-withdrawing effect, yielded remarkable functionalization results, reaching up to 21.8 wt%. Diazonium compounds containing halogen or neutral groups provided intermediate yields when compared to the more typical donating or withdrawing groups, with results as follows: Br (8.1 wt%), F (8.2 wt%), and naphthalene (13.8 wt%). The complete analysis of functionalized BNNT was depicted in ESI Fig. 1–3.†
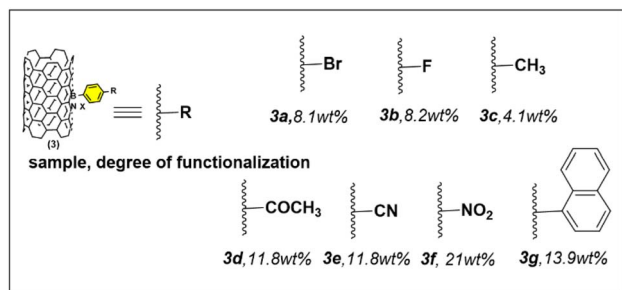
Attachment of aromatic ring on the surface of BNNT and starting material were re-dispersed in common solvents, such as isopropanol (IPA), acetone N,N′-dimethyl formamide (DMF), and tetrahydrofuran (THF) then presented in Fig. 7. The dispersion information was also supported by UV-Vis estimation method at 500 nm wavelength (depicted in ESI Fig. 4†). As previously reported, BNNT exhibit temporary dispersion in water and alcohols using high-energy sonication,[53] therefore, isopropanol is chosen as the first dispersion environment. In Fig. 7a, it is evident that samples 3a–3g, excluding 3d, exhibit improved dispersions upon visual inspection. As per observation ESI Fig. 4a,† after 2 days of dispersion, the original sample settled nearly completely, with an absorbance of approximately 8.24×10^{-4} absorbance units (a.u). Conversely, the functionalized samples demonstrated stable dispersions over several days, with absorbance levels ranging from 0.0175 a.u to 0.11 a.u. This suggests a significant enhancement in dispersibility for the functionalized samples in isopropanol, estimated to be between 21 (3e) and 133 times (3c) greater than the original sample.

A recent article reported that N,N′-dimethyl formamide is a good solvent for BNNT dispersion with a sedimentation time of up to 42.6 hours.[54] Indeed, the picture of the dispersions (Fig. 7c) shows BNNT/DMF progressively lost part or all of their stability and almost went down over time. On the contrary, samples 3a to 3d exhibit excellent dispersion behavior when subjected to higher energy conditions. The dispersibility varies from 2 to 36 times, with sample 3f demonstrating a factor of 2 and sample 3c showing a factor of 36, as detailed in ESI Fig. 4c.† Acetone and THF are both recognized as poor dispersion systems for BNNT. Intriguingly, the results depicted in Fig. 7b illustrate the dispersion observed after 48 hours for samples 3a to 3c, whereas all samples demonstrate superior dispersion properties in Fig. 7d compared to non-functionalized BNNT. The dispersibility increases from 2 (3b) to 37 (3g) times in the case of acetone and from 1.2 (3g) to 14.5 (3a) in the case of THF, as outlined in ESI Fig. 4b and d.† The instability of BNNT is caused by a substantial polarity difference between the nanotubes and the solvent. BN structures have a dipolar moment due to the difference in electronegativity between B and N atoms. However, the attachment of organic molecules to the surface might modify the polarity of the BNNT, resulting in high solubility in solvents such as acetone or THF.
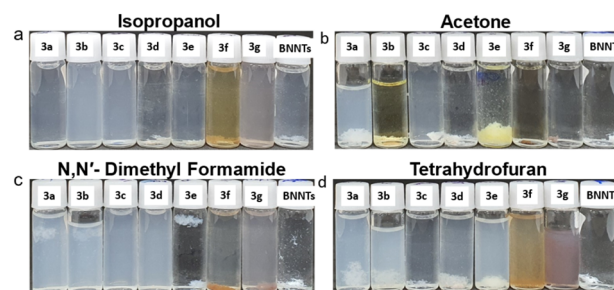

Fig. 6 Substrate scope.

Fig. 7 Photos of 3a–3g re-dispersed in various solvents (a) isopropanol (b) acetone (c) N,N′-dimethyl formamide (d) tetrahydrofuran. Left to right: 3a–3g and BNNT/solvent (after 48 h).

The way a material disperses can be influenced by various factors such as its initial structure, the type of solvent chosen, and the structure of the group attached to the surface, including the influence of the functional groups. Additionally, the amount of surfactants can also play a role. However, it can be difficult to accurately analyze the impact of each component. Nonetheless, in this context, we can get some insight into the influence of functional groups on dispersion in suitable solvents. Nonpolar groups like F, Br, CH_3, and Naphthalene tend to disperse well in a wide range of solvents compared to polar functional groups like CN, NO_2, and $COCH_3$. This suggests that there may be intermolecular interactions at play. For instance, highly polar groups can coordinate with N or B atoms in another nanotube, leading to aggregation and decreased dispersibility of the functionalized nanotube.

Lastly, it is crucial to ensure that BNNTs remain well-dispersed without any precipitation over the period, as this is essential for their effective application. Fig. 8 presents the results of a long-term stability assessment of the functionalized BNNT (3a–3g), as well as BNNT analyzed using the absorbance value from UV-Vis spectra.[55] All analyses (Fig. 8a–d) exhibit a consistent trend: pristine BNNT solutions degrade in stability more rapidly than functionalized BNNT under identical measurement conditions. Within 48 hours, the dispersibility decay rate (DDR) for BNNT reached up to 80% in isopropanol (IPA), nearly 100% in acetone, 62% in dimethylformamide (DMF), and 75% in tetrahydrofuran (THF). In contrast, all functionalized samples demonstrated significantly improved stability, maintaining a DDR below 30% after 2 days. Specifically, in IPA, the DDR ranged from 4.3% to 17.8%, with a minimum of 4.4% for sample 3c and a maximum of 17.8% for sample 3b. For acetone, the DDR reached up to 17% for sample 3d, with a minimum of 3.9% for sample 3f. In DMF, the DDR varied from 11.5% for sample 3c to 26.5% for sample 3f. Finally, in THF, the DDR ranged from 7.6% for sample 3b to 17.7% for sample 3d.
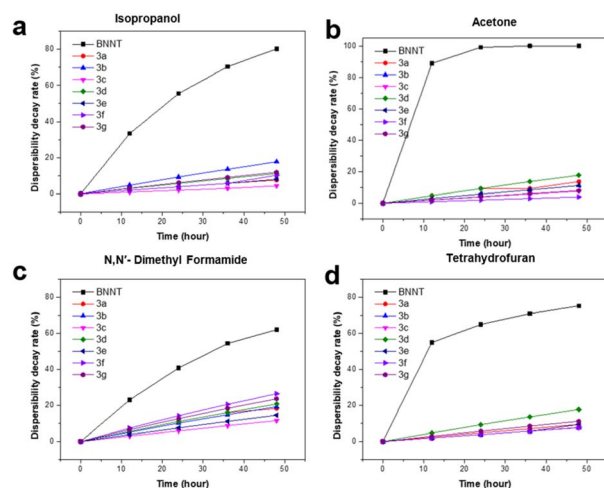

Fig. 8 Dispersibility decay rate estimated from UV-Vis at 500 nm of 3a–3g re-dispersed in various solvents (a) isopropanol (b) acetone (c) N,N′-dimethyl formamide (d) tetrahydrofuran.

Experimental

Materials

As-synthesized BNNT was supplied by the High-Enthalpy Plasma Research Center at Jeonbuk National University (Republic of Korea). Diazonium salts were purchased from Sigma-Aldrich. Solvents were obtained from Daejung Chemicals. All chemicals are used without further purification.

Synthesis procedure

Purification of BNNT before using in reaction. The as-synthesized BNNT were then purified to remove the amorphous element boron according to the method described elsewhere.[56,57] First, the sample was annealed in the furnace at 650 °C for oxidation of amorphous boron to boron trioxide. Calcined BNNT were washed with DI water several times every 30 minutes to remove boron oxides and filtered to collect BNNT.

Synthesis of functionalized BNNT. In a 30 ml vial, 10 mg pretreated BNNT in 10 ml solvent was placed, then the mixture was bath sonicated (Portable Ultrasonic Cleaner (JAC-3010) equipment at high frequency) for 60 min at room temperature to disperse the tubes in solution. A magnetic stir bar was added to the vial along with 100 mg diazonium salt and immediately clamped into a silicone oil bath set to 55 °C, then the mixture was stirred for an additional 16 hours. The product was washed with deionized water, acetone, methylene chloride, and methanol successively, followed by the treatment of ultrasonic and centrifugation to remove the extra salt. The resultant product was dried at 80 °C for 24 h in a vacuum oven.

Characterization

Fourier transform infrared spectroscopy (FTIR) was carried out using Nicolet iS10 instrument (ThermoFisher Scientific) Infrared Spectrum Analyzer in the 4000–500 cm^{-1} wave number range with KBr pellets. Thermal gravimetric analysis (TGA) was carried out using Rigaku Thermo Plus EVO2 by increasing the temperature up to 900 °C (ramp: 10 °C min^{-1}) under flowing air (60 ml min^{-1}). X-ray photoelectron spectroscopy (XPS) was measured with photoelectron spectrometer (K-alpha, Thermo Fisher) with an excitation source used for survey spectra was by standard Al Kα (1486.6 eV) at 14.9 keV anode voltage. The filament current was 4.6 A, and the emission current was 20 mA. Transmission electron microscopy (TEM) (Technai G2 F20, FEI, Hillsboro, OR, USA) at 200 kV. Scanning electron microscope (SEM) was carried out on a high-resolution scanning electron microscope (SEM NovaFEI). All SEM samples were prepared by filtering the dispersion suspension on the PVDF membrane (Durapore, 0.22 μm). UV-670 UV-Vis Spectrophotometer from Jasco was used to estimate the dispersion of BNNT.

Conclusions

The research described attempts to enhance BNNT surface functionality and processability concerning dispersibility in organic solvents. It demonstrated a novel, facile, and straightforward method for producing chemically functionalized boron

nitride nanotubes. A mechanistic study was also conducted that revealed that the electrons' localization into the empty B-centered orbitals of the BNNT plays an important role in the enhanced reactivity by promoting covalent bond formation with the electrons in the carbocation. The attachment of various groups of aromatic moieties was carefully characterized using microscopy, spectroscopy, and thermal measurement, providing evidence of covalent functionalization. Interestingly, most of the functionalized BNNT described here exhibit well-dispersibility and long last for more than a few days. Successfully grafting reactive functionalities, such as terminal benzene rings or functional groups enables additional chemical modification, including covalent insertion into polymer networks or various materials. This, in turn, may significantly increase BNNT compatibility in polymer matrix, enabling the production of high-performance BNNT–polymer composites or fiber.

Data availability

The data supporting this article have been included as part of the ESI.†

Author contributions

T. Q. H.: conceptualization, validation, investigation, writing – original draft; M. S. K.: investigation; J. G. K. and S. H. A.: supervision, writing – review & editing. All authors have read and agreed to the published version of the manuscript.

Conflicts of interest

There are no conflicts to declare.

Acknowledgements

References

1 A. Rubio, J. L. Corkill and M. L. Cohen, *Phys. Rev. B: Condens. Matter Mater. Phys.*, 1994, **49**, 5081–5084.

2 N. G. Chopra, R. J. Luyken, K. Cherrey, V. H. Crespi, M. L. Cohen, S. G. Louie and A. Zettl, *Science*, 1995, **269**, 966–967.

3 J. H. Kim, T. V. Pham, J. H. Hwang, C. S. Kim and M. J. Kim, *Nano Convergence*, 2018, **5**, 17.

4 W.-Q. Han and A. Zettl, *J. Am. Chem. Soc.*, 2003, **125**, 2062–2063.

5 R. Arenal, M.-S. Wang, Z. Xu, A. Loiseau and D. Golberg, *Nanotechnology*, 2011, **22**, 265704.

6 E. Hernández, C. Goze, P. Bernier and A. Rubio, *Phys. Rev. Lett.*, 1998, **80**, 4502–4505.

7 A. P. Suryavanshi, M.-F. Yu, J. Wen, C. Tang and Y. Bando, *Appl. Phys. Lett.*, 2004, **84**, 2527–2529.

8 N. G. Chopra and A. Zettl, *Solid State Commun.*, 1998, **105**, 297–300.

9 C. W. Chang, A. M. Fennimore, A. Afanasiev, D. Okawa, T. Ikuno, H. Garcia, D. Li, A. Majumdar and A. Zettl, *Phys. Rev. Lett.*, 2006, **97**, 085901.

10 D. A. Stewart, I. Savić and N. Mingo, *Nano Lett.*, 2009, **9**, 81–84.

11 C. Zhi, Y. Bando, T. Terao, C. Tang, H. Kuwahara and D. Golberg, *Adv. Funct. Mater.*, 2009, **19**, 1857–1862.

12 X. Blase, A. Rubio, S. G. Louie and M. L. Cohen, *Europhys. Lett.*, 1994, **28**, 335–340.

13 J. S. Lauret, R. Arenal, F. Ducastelle, A. Loiseau, M. Cau, B. Attal-Tretout, E. Rosencher and L. Goux-Capes, *Phys. Rev. Lett.*, 2005, **94**, 037405.

14 Y. Chen, J. Zou, S. J. Campbell and G. Le Caer, *Appl. Phys. Lett.*, 2004, **84**, 2430–2432.

15 H. Shin, J. Guan, M. Z. Zgierski, K. S. Kim, C. T. Kingston and B. Simard, *ACS Nano*, 2015, **9**, 12573–12582.

16 D. Golberg, Y. Bando, Y. Huang, T. Terao, M. Mitome, C. Tang and C. Zhi, *ACS Nano*, 2010, **4**, 2979–2993.

17 L. Zhao, C. Wei, Z. Li, W. Wei, L. Jia, X. Huang, W. Ning, Z. Wang and J. Ren, *Mater. Des.*, 2021, **210**, 110124.

18 K. C. Yung, T. Xu and H. S. Choy, *J. Mater. Sci.: Mater. Electron.*, 2016, **27**, 5217–5224.

19 Y. Jia, T. D. Ajayi, J. Morales, M. A. R. Chowdhury, G. Sauti, S.-H. Chu, C. Park and C. Xu, *J. Am. Ceram. Soc.*, 2019, **102**, 7584–7593.

20 J. Shu, R. Xia, J. Qian, J. Miao, L. Su, M. Cao, H. Lin, P. Chen and J. Chen, *Macromol. Res.*, 2016, **24**, 640–644.

21 M. C. Vu, T. S. Tran, Y. H. Bae, M. J. Yu, V. C. Doan, J. H. Lee, T. K. An and S.-R. Kim, *Macromol. Res.*, 2018, **26**, 521–528.

22 X. Zeng, J. Sun, Y. Yao, R. Sun, J.-B. Xu and C.-P. Wong, *ACS Nano*, 2017, **11**, 5167–5178.

23 X. Chen, C. M. Dmuchowski, C. Park, C. C. Fay and C. Ke, *Sci. Rep.*, 2017, **7**, 11388.

24 S.-H. Lee, M. J. Kim, S. Ahn and B. Koh, *Int. J. Mol. Sci.*, 2020, **21**, 1529.

25 X. Chen, P. Wu, M. Rousseas, D. Okawa, Z. Gartner, A. Zettl and C. R. Bertozzi, *J. Am. Chem. Soc.*, 2009, **131**, 890–891.

26 G. Ciofani, S. Danti, G. G. Genchi, B. Mazzolai and V. Mattoli, *Small*, 2013, **9**, 1672–1685.

27 M. Ghazizadeh, J. Estevez and A. Kelkar, *Int. J. Nano Stud. Technol.*, 2015, **4**(01e), 1–2.

28 D.-H. Kim, H.-K. Jang, M.-S. Kim, S.-D. Kim, D.-J. Lee and G. T. Kim, *Phys. Chem. Chem. Phys.*, 2017, **19**, 976–985.

29 C. Ban, L. Li and L. Wei, *RSC Adv.*, 2018, **8**, 29141–29146.

30 D. Zhang, S. Zhang, N. Yapici, R. Oakley, S. Sharma, V. Parashar and Y. K. Yap, *ACS Omega*, 2021, **6**, 20722–20728.

31 C. H. Lee, D. Zhang and Y. K. Yap, *J. Phys. Chem. C*, 2012, **116**, 1798–1804.

32 S. Velayudham, C. H. Lee, M. Xie, D. Blair, N. Bauman, Y. K. Yap, S. A. Green and H. Liu, *ACS Appl. Mater. Interfaces*, 2010, **2**, 104–110.

33 V. Piazza and M. Gemmi, in *Boron Nitride Nanotubes in Nanomedicine*, ed. G. Ciofani and V. Mattoli, William Andrew Publishing, Boston, 2016, pp. 139–147.

34 S. Behzad, *Superlattices Microstruct.*, 2015, **82**, 630–638.

35 N. Yanar, E. Yang, H. Park, M. Son and H. Choi, *Membranes*, 2020, **10**, 430.

36 C. S. T. Castillo, C. Bruel and J. R. Tavares, *Nanoscale Adv.*, 2020, **2**, 2497–2506.

37 Z. Hanif, K.-I. Choi, J.-H. Jung, A. G. M. Pornea, E. Park, J. Cha, H.-R. Kim, J.-H. Choi and J. Kim, *Ind. Eng. Chem. Res.*, 2023, **62**, 2662–2670.

38 A. L. Tiano, C. Park, J. W. Lee, H. H. Luong, L. J. Gibbons, S.-H. Chu, S. Applin, P. Gnoffo, S. Lowther, H. J. Kim, P. M. Danehy, J. A. Inman, S. B. Jones, J. H. Kang, G. Sauti, S. A. Thibeault, V. Yamakov, K. E. Wise, J. Su and C. C. Fay, Nanosensors, Biosensor and Info-Tech Sensors and Systems, *SPIE*, 2014, 9060, pp. 1–9.

39 K. K. Smith, N. D. Redeker, J. C. Rios, M. H. Mecklenburg, J. C. Marcischak, A. J. Guenthner and K. B. Ghiassi, *ACS Appl. Nano Mater.*, 2019, **2**, 4053–4060.

40 Z. Wang, Q. Li, J. Liu, H. Li and S. Zheng, *J. Nanomater.*, 2018, **2018**, e6717046.

41 A. O. Maselugbo, J. E. Knoop, K. S. Nowlin, G. Pathiraja, H. B. Harrison and J. R. Alston, *J. Mater. Res.*, 2022, **37**, 4496–4507.

42 R. Iannitto, H. Shin, Y. Martinez Rubi, B. Simard and S. Coulombe, *ACS Appl. Nano Mater.*, 2020, **3**, 294–302.

43 C. S. Torres-Castillo and J. R. Tavares, *Can. J. Chem. Eng.*, 2023, **101**(3), 1410–1420.

44 H. Shin, J. Guan, M. Z. Zgierski, K. S. Kim, C. T. Kingston and B. Simard, *ACS Nano*, 2015, **9**, 12573–12582.

45 G. Ciofani, G. G. Genchi, I. Liakos, A. Athanassiou, D. Dinucci, F. Chiellini and V. Mattoli, *J. Colloid Interface Sci.*, 2012, **374**, 308–314.

46 S. Lin, B. Ashrafi, K. Laqua, K. S. Kim and B. Simard, *New J. Chem.*, 2017, **41**, 7571–7577.

47 K. K. Smith, N. D. Redeker, J. C. Rios, M. H. Mecklenburg, J. C. Marcischak, A. J. Guenthner and K. B. Ghiassi, *ACS Appl. Nano Mater.*, 2019, **2**, 4053–4060.

48 C. A. de los Reyes, K. L. Walz Mitra, A. D. Smith, S. Yazdi, A. Loredo, F. J. Frankovsky, E. Ringe, M. Pasquali and A. A. Martí, *ACS Appl. Nano Mater.*, 2018, **1**, 2421–2429.

49 I. Bravo, T. García-Mendiola, M. Revenga-Parra, F. Pariente and E. Lorenzo, *Sens. Actuators, B*, 2015, **211**, 559–568.

50 J. L. Bahr, J. Yang, D. V. Kosynkin, M. J. Bronikowski, R. E. Smalley and J. M. Tour, *J. Am. Chem. Soc.*, 2001, **123**, 6536–6542.

51 J. Lee, B. Hong and A. Lee, *J. Org. Chem.*, 2019, **84**, 9297–9306.

52 M. S. Strano, C. A. Dyke, M. L. Usrey, P. W. Barone, M. J. Allen, H. Shan, C. Kittrell, R. H. Hauge, J. M. Tour and R. E. Smalley, *Science*, 2003, **301**, 1519–1522.

53 C. H. Lee, D. Zhang and Y. K. Yap, *J. Phys. Chem. C*, 2012, **116**, 1798–1804.

54 C. S. T. Castillo, C. Bruel and J. R. Tavares, *Nanoscale Adv.*, 2020, **2**, 2497–2506.

55 S.-W. Jeon, S. C. Kang, H. Choi, H. I. Yoo, S. Y. Moon and T.-H. Kim, *ACS Appl. Nano Mater.*, 2024, **7**, 394–403.

56 S.-H. Lee, M. Kang, H. Lim, S. Y. Moon, M. J. Kim, S. G. Jang, H. J. Lee, H. Cho and S. Ahn, *Appl. Surf. Sci.*, 2021, **555**, 149722.

57 J. Ko, H. M. Kim, S. Y. Moon, S. Ahn, S. G. Im and Y. Joo, *Chem. Mater.*, 2021, **33**, 4723–4732.